
Sparse Grouped Gaussian Processes for Solar Power Forecasting

Astrid Dahl
University of New South Wales
Sydney

Edwin V. Bonilla
Data 61
Sydney

Abstract

We consider multi-task regression models where observations are assumed to be a linear combination of several latent node and weight functions, all drawn from Gaussian process priors that allow nonzero covariance between *grouped* latent functions. Motivated by the problem of developing scalable methods for distributed solar forecasting, we exploit sparse covariance structures where latent functions are assumed to be conditionally independent given a group-pivot latent function. We exploit properties of multivariate Gaussians to construct sparse Cholesky factors directly, rather than obtaining them through iterative routines, and by doing so achieve significantly improved time and memory complexity including prediction complexity that is linear in the number of grouped functions. We test our approach on large multi-task datasets and find that sparse specifications achieve the same or better accuracy than non-sparse counterparts in less time, and improve on benchmark model accuracy.

1 INTRODUCTION

The problem of forecasting local solar output in the short term is of significant interest for the purpose of distributed grid control and household energy management [31, 33]. A number of studies confirm that exploiting spatial dependencies between proximate sites can yield significant gains in forecast accuracy and stability [10, 36]. More importantly, inherent to this application is the need for modeling uncertainty in a flexible and principled way [4].

Gaussian process (GP) models are a flexible nonparametric Bayesian approach that can be applied to various problems such as regression and classification [22] and have

been extended to numerous multivariate and multi-task problems including spatial and spatio-temporal contexts [7]. Multi-task GP methods have been developed along several lines [see e.g. 3, for a review] including mixing approaches that combine multiple latent univariate Gaussian processes via linear or nonlinear mixing to predict multiple related tasks [5, 10, 14, 17, 28, 35]. To maintain scalability in multi task mixing models, various constraints have been employed. In particular, latent Gaussian processes may be constrained to be statistically independent as in [11, 35] or covarying with constrained kernel structures to allow algebraic efficiencies as in [5, 10].

Recently there has been renewed interest in sparse GP models and low rank approximations to reduce the complexity of computing the required Cholesky factor components that are a key limitation on complexity in most GP methods [8, 13, 34].

In this paper we consider the case where subsets of latent functions in Gaussian process regression networks [GPRN; 35] covary within a constrained structure. We follow the grouped Gaussian process (GGP) approach of [10], where groups of latent functions may covary arbitrarily with a separable kernel structure. Posterior estimation in this GGP framework, as originally proposed in [10], is underpinned by variational inference based on inducing variables [30], hence it should be inherently scalable to a large number of observations. However, both the time and space complexity deteriorate significantly when considering a large number of tasks, due to the assumed grouping structure.

Therefore, to address the above limitation, in this paper we consider the case where grouped functions are conditionally independent given a specific group-dependent *pivot* function. With this, we exploit known properties of the multivariate normal distribution to induce spatially-driven sparsity in the cross function precision matrix and the Cholesky factor of the corresponding covariance. Furthermore, such a modeling assumption allows us to construct

these matrices directly using explicit analytical expressions, eliminating the usual need to obtain them through costly and potentially numerically unstable routines with cubic complexity on the number of latent functions. Finally, we extend the use of sparse structures to the corresponding approximate distributions within a variational inference framework. The required expectation over these variational distributions are neatly estimated using a simple but effective ‘indirect’ sampling approach from the latent posterior distributions, which further improve scalability on the number of functions.

We apply our approach to the problem of forecasting solar power output at multiple distributed sites in Australia using two large multi-task datasets. Our results show that sparse specifications achieve the same or better forecast accuracy and variance than non-sparse counterparts in less time, and improve on benchmark model accuracy.

2 RELATED WORK

Since the development of sparse variational GP methods as in [16, 30] a number of recent works have sought to reduce complexity of GP models by inducing sparsity in covariance or precision matrices. These approaches include assuming conditional independence between functions at points or subsets of points, imposing structure on input points and low rank approximations, and more recently combinations of these ideas.

Numerous earlier methods sought to exploit sparsity in precision or Cholesky matrices by inducing conditional independence constraints. In general these methods approximate the full covariance matrix for a positive definite kernel with $\mathbf{K}_{\mathbf{x}\mathbf{x}}^r \approx \mathbf{K}_{\mathbf{x},\tilde{\mathbf{x}}} \mathbf{K}_{\tilde{\mathbf{x}},\tilde{\mathbf{x}}}^{-1} \mathbf{K}_{\tilde{\mathbf{x}},\mathbf{x}}$ where $\tilde{\mathbf{x}}$ may be some subset of inputs or inducing points, potentially with some diagonal correction (also termed ‘preconditioning’) to ensure nondegeneracy, as in early sparse methods such as FITC or PITC [20, 24]. Later studies build on the PITC approach to extend conditional independence concepts to convolutional multi-task models and the variational inference setting [1, 2].

Other methods make use of conditional independence relationships arising naturally in Gaussian Markov random field (UGM) models, particularly the Integrated Nested Laplace method (INLA) of Rue et al. [23]. The models in these case assumes a more general conditional independence structure arising from the Markov blanket property in such models (as do [1, 2]). As in the approach proposed here, this property induces sparsity in the precision matrix and Cholesky factor. Another idea that has been utilized in sparse methods is that of structured inputs e.g. regular one-dimensional gridded inputs, which induce Toeplitz matrices with sparse inverses. The GP-KISS approach in

[34] exploits gridded inputs in combination with low rank approximations to develop fast, conjugate gradient based methods.

Closely related to methods inducing conditional independence, several recent methods consider low rank approximations of $\mathbf{K}_{\mathbf{x}\mathbf{x}}^r$ in inducing point frameworks [9, 13]. Gardner et al. [13] use a low-rank pivoted Cholesky approximation with pre-conditioning in combination with iterative methods to estimate key terms appearing in the objective function for various GP models including sparse methods. Other approaches using low-rank approximations based on spectral methods have also been proposed as in [12, 25].

While sparse variational and other recent low-rank GP methods have provided substantial gains in scalability in recent years, as general approaches they do not necessarily exploit efficiencies where sparse, cross-task covariances can be specified *a priori* as may be possible in well understood spatiotemporal problems.

3 MULTI TASK GP REGRESSION

A Gaussian process [GP; 22] is formally defined as a distribution over functions such that $f(\mathbf{x}) \sim \mathcal{GP}(\mu(\mathbf{x}), \kappa(\mathbf{x}, \mathbf{x}'))$ is a Gaussian process with mean function $\mu(\mathbf{x})$ and covariance function $\kappa(\mathbf{x}, \mathbf{x}')$ iff any subset of function values $f(\mathbf{x}_1), f(\mathbf{x}_2), \dots, f(\mathbf{x}_N)$ follows a Gaussian distribution with mean $\boldsymbol{\mu}$ and covariance \mathbf{K} , which are obtained by evaluating the corresponding mean function and covariance function at the input points $\mathbf{X} = \{\mathbf{x}_1, \dots, \mathbf{x}_N\}$.

In this paper we consider a form of multi-task GP regression where multiple outputs are modeled as a linear combination of node and weight functions, each of which is a GP. Data is of the form $\mathcal{D} = \{\mathbf{X} \in \mathbb{R}^{N \times D}, \mathbf{Y} \in \mathbb{R}^{N \times P}\}$ where each $\mathbf{x}_{(n)}$ in \mathbf{X} is a D -dimensional vector of input features and each $\mathbf{y}_{(n)}$ in \mathbf{Y} is a P -dimensional vector of task outputs. We consider the grouped Gaussian process (GGP) model of [10] who place a prior over Q latent GP functions $\mathbf{F} = \{f_j(\mathbf{x})\}_{j=1}^Q$ such that arbitrary, non-overlapping subsets (‘groups’) of latent functions may have nonzero covariance.

We denote arbitrarily chosen subsets in \mathbf{F} as $\mathbf{F}_r \in \mathbb{R}^{N \times Q_r}$, $r = 1, \dots, R$, where R is the total number of groups. For each group the number of latent functions within is denoted Q_r (group size) such that $\sum_{r=1}^R Q_r = Q$. In the GGP each group is comprised of latent functions $\mathbf{F}_r = \{f_j\}_{j \in \text{group } r}$ and the covariance between two functions is non-zero iff the corresponding processes belong to the same group. This leads to a prior over functions

given by

$$p(\mathbf{F}|\boldsymbol{\theta}) = \prod_{r=1}^R p(\mathbf{F}_r|\boldsymbol{\theta}_r) = \prod_{r=1}^R \mathcal{N}(\mathbf{F}_r; \mathbf{0}, \mathbf{K}_{ff}^r), \quad (1)$$

where $\mathbf{K}_{ff}^r \in \mathbb{R}^{NQ_r \times NQ_r}$ is the covariance matrix generated by the group kernel function $\kappa_r(f_j(\mathbf{x}), f_{j'}(\mathbf{x}'))$, which evaluates the covariance of functions f_j and $f_{j'}$ at the locations \mathbf{x} and \mathbf{x}' , respectively. $\kappa_r(f_j(\mathbf{x}), f_{j'}(\mathbf{x}')) = 0$ iff the functions f_j and $f_{j'}$ do not belong to the same group r .

Correlations between outputs are modeled as in the Gaussian process regression network (GPRN) likelihood of Wilson et al. [35], where

$$\begin{aligned} p(\mathbf{Y}|\mathbf{F}, \phi) &= \prod_{n=1}^N p(\mathbf{y}_{(n)}|\mathbf{f}_{(n)}, \phi) \\ &= \prod_{n=1}^N \mathcal{N}(\mathbf{y}_{(n)}; \mathbf{W}_{(n)}\mathbf{g}_{(n)}, \boldsymbol{\Sigma}_y). \end{aligned} \quad (2)$$

Here we define \mathbf{W} and \mathbf{G} subsets of \mathbf{F} formed by gathering PQ_g and Q_g functions in \mathbf{F} , respectively, with $Q_g(P+1) = Q$, $\phi = \boldsymbol{\Sigma}_y$, $\mathbf{f}_{(n)} = \{\mathbf{W}_{(n)}, \mathbf{g}_{(n)}\}$ and $\boldsymbol{\Sigma}_y$ is a diagonal matrix. P -dimensional outputs are thus constructed at $\mathbf{x}_{(n)}$ as the product of a $P \times Q_g$ matrix of weight functions, $\mathbf{W}_{(n)}$, and Q_g -dimensional vector of node functions $\mathbf{g}_{(n)}$. We note that in the approach of [10], which builds on the generic inference method allowing ‘black box’ likelihoods of [11], partitions of \mathbf{F} with respect to \mathbf{W} and \mathbf{G} need not align with partitions into groups \mathbf{F}_r . Hence grouping in the prior can be independent of the likelihood definition and, for brevity, inference is presented below simply in terms of \mathbf{F} and \mathbf{F}_r rather than \mathbf{W} and \mathbf{G} .

To maintain scalability of the approach, the model of [10] considers separable kernels of the form $\kappa_r(f_j(\mathbf{x}), f_{j'}(\mathbf{x}')) = \kappa_r(\mathbf{x}, \mathbf{x}')\kappa_r(\mathbf{h}_j, \mathbf{h}_{j'})$, where for each group Q_r vectors $\mathbf{h} \in H$ form a feature matrix $\mathbf{H}_r \in \mathbb{R}^{Q_r \times H}$ that governs covariance across functions $\mathbf{f}_j \in \mathbf{F}_r$. Group covariance $\mathbf{K}_{ff}^r = \mathbf{K}_{hh}^r \otimes \mathbf{K}_{xx}^r$ thus decomposes into $\mathbf{K}_{xx}^r \in \mathbb{R}^{N \times N}$ and $\mathbf{K}_{hh}^r \in \mathbb{R}^{Q_r \times Q_r}$.

In this paper we propose sparse forms of \mathbf{K}_{hh}^r arising from a constrained form of cross-function covariance, whereby functions within a group are conditionally independent given a group ‘pivot’ latent function. By exploiting conditional independence constraints that can reasonably fit with spatiotemporal applications such as distributed solar prediction (rationale are discussed further in §6), it is possible to dramatically reduce the complexity of the GGP with respect to group size. This is possible due to properties of multivariate Gaussians that allow

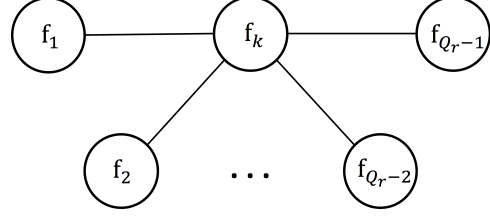


Figure 1: Example of Undirected Graphical Model in Star Formation for $\mathbf{F}_r = (f_1, f_2, \dots, f_{Q_r})'$.

direct construction of sparse precision and Cholesky factor matrices as discussed below. We do not propose the same form of sparsity for \mathbf{K}_{xx}^r as in the context of spatiotemporal modelling the implied temporal conditional independence constraints in that case become problematic.

Since spatial feature matrix \mathbf{H}_r and hence \mathbf{K}_{hh}^r are constant across observations $\mathbf{x}_{(n)}$, we also consider the case where \mathbf{K}_{hh}^r is freely parameterized rather than feature-dependent.

4 SPARSE MULTI TASK MODEL

In this section we describe the main assumptions on the task-dependent covariance of our sparse GGP model that will yield significant computational gains over the original GGP. The starting point is that of conditional independence across functions given a group-*pivot* latent function.

4.1 CONDITIONAL INDEPENDENCE

When variables are jointly normally distributed and subsets of these variables are conditionally independent, their multivariate normal distribution is known to have certain useful properties. Suppose variables $\mathbf{F}_r = f_1, f_2, \dots, f_{Q_r}$ are jointly normally distributed with covariance \mathbf{K} (subscripts on \mathbf{K} are dropped for ease of exposition), and suppose that, given some variable f_k , the remaining variables are conditionally independent. That is,

$$\begin{aligned} \mathbf{F}_r &\sim \mathcal{N}(\boldsymbol{\mu}, \mathbf{K}) \quad \text{and} \\ f_i &\perp f_j \mid f_k, \quad \forall \quad i, j \neq k, \quad i \neq j \end{aligned} \quad (3)$$

where $f_i \perp f_j \mid f_k$ denotes independence of f_i and f_j given f_k . This joint distribution can be represented as a ‘star’ or ‘tree’ undirected graphical model, where f_k can be conceived as a ‘pivot’ variable connecting all other variables (Figure 1). Where variables are jointly distributed according to (3), known, sparse expressions for the Cholesky factor and inverse covariance, that allow

direct construction of these matrices, can be obtained analytically [26, 27, 32]. Specifically, for $i, j \neq k, i \neq j$, the covariance element $\mathbf{K}_{i,j} = \text{Cov}(f_i, f_j)$ is given by

$$\begin{aligned} \mathbf{K}_{i,j} &= \mathbf{K}_{i,k} \mathbf{K}_{k,k}^{-1} \mathbf{K}_{k,j} \iff f_i \perp f_j \mid f_k, \\ \text{leading to } \Phi_{i,j} &= 0, \\ \text{and } \Lambda_{i,j} &= 0 \end{aligned} \quad (4)$$

where Λ and Φ are the precision matrix and lower triangular Cholesky factor associated with \mathbf{K} . This result also holds for the multivariate analogue where, for example, \mathbf{F}_r is partitioned into subsets $(\mathbf{F}_{Q_r,1}, \mathbf{F}_{Q_r,2}, \dots)$ in which case $\mathbf{K}_{i,j} = \text{Cov}(\mathbf{F}_i, \mathbf{F}_j)$ represents a submatrix, and similar for $\Phi_{i,j}$ and $\Lambda_{i,j}$.

Moreover, nonzero elements of Λ and Φ have a known form [see, e.g. 26, 27]. Without loss of generality, where f_2, \dots, f_{Q_r} are conditionally independent given f_1 , the precision matrix takes a winged-diagonal form (see the Supplement) where all elements (or submatrices, where \mathbf{F}_r is partitioned into subsets rather than individual variables) have forms:

$$\begin{aligned} \Lambda_{11} &= \mathbf{K}_{11}^{-1} + \sum_{i=2}^{Q_r} \mathbf{K}_{11}^{-1} \mathbf{K}_{1i} \mathbf{K}_{ii,1}^{-1} \mathbf{K}_{i1} \mathbf{K}_{11}^{-1} \\ \Lambda_{i1} &= -\mathbf{K}_{11}^{-1} \mathbf{K}_{1i} \mathbf{K}_{ii,1}^{-1}, \quad \text{and} \quad \Lambda_{ii} = \mathbf{K}_{ii,1}^{-1}, \quad \text{with} \\ \mathbf{K}_{ii,1}^{-1} &= \mathbf{K}_{ii} - \mathbf{K}_{i1} \mathbf{K}_{11}^{-1} \mathbf{K}_{1i}, \quad i = 2, \dots, Q_r \end{aligned} \quad (5)$$

Of key importance for our model, the associated Cholesky lower triangular factor Φ has a known, sparse form where $\Phi_{11} = \text{Chol}(\mathbf{K}_{11})$, $\Phi_{i1} = \mathbf{K}_{i1}(\Phi_{11})^{-1}$, $i = 2, \dots, Q_r$ and $\Phi_{ii} = \text{Chol}(\mathbf{K}_{ii,1}^{-1})$, $i = 2, \dots, Q_r$, and all other elements are zero. Here the operator $\text{Chol}(\cdot)$ denotes the Cholesky factorization of the given argument.

4.2 SPARSE GAUSSIAN PROCESS

Let $f(\mathbf{h})$ be drawn from a Gaussian process, $f(\mathbf{h}) \sim \mathcal{GP}(\mathbf{0}, \kappa(\mathbf{h}, \mathbf{h}'))$ and assume that $f(\mathbf{h}_i) \perp f(\mathbf{h}_j) \mid f(\mathbf{h}_k)$ for some $i, j \neq k, i \neq j$. Thus, the properties of multivariate Gaussians above imply the constrained covariance form

$$\kappa(\mathbf{h}_i, \mathbf{h}_j) \equiv \kappa(\mathbf{h}_i, \mathbf{h}_k) \kappa(\mathbf{h}_k, \mathbf{h}_j)^{-1} \kappa(\mathbf{h}_k, \mathbf{h}_j). \quad (6)$$

Again without loss of generality, setting $k = 1$ and $i = 2, \dots, Q_r$ yields a sparse form of the Cholesky factor where

$$\begin{aligned} \Phi_{11} &= \text{Chol}(\kappa_{11}), \quad \Phi_{i1} = \kappa_{i1}(\Phi_{11})^{-1}, \quad \text{and} \\ \Phi_{ii} &= \text{Chol}(\kappa_{ii} - \kappa_{i1} \kappa_{11}^{-1} \kappa_{1i}). \end{aligned} \quad (7)$$

This form has several useful characteristics. Computation involves only univariate operations, meaning that

$\text{Chol}(\cdot) = \sqrt{(\cdot)}$, $(\Phi_{11})^{-1} = \frac{1}{\Phi_{11}}$ and $\kappa_{11}^{-1} = \frac{1}{\kappa_{11}}$. Since there are $2Q_r - 1$ nonzero terms, complexity of both computation and storage is $\mathcal{O}(Q_r)$ rather than the more general $\mathcal{O}(Q_r^3)$ and $\mathcal{O}(Q_r^2)$. Computation involving univariate operations only also allows direct control over numerical stability of the factorization.

In addition, the sparse form can be decomposed as two sparse matrices with a single nonzero column and nonzero diagonal respectively, i.e.

$$\Phi = [\Phi_{\cdot,1}, \mathbf{0}_1, \dots, \mathbf{0}_{Q_r-1}] + \text{diag}(0, \Phi_{22}, \dots, \Phi_{Q_r Q_r}).$$

where $[\cdot]$ is the concatenation of the first column of Φ ($\Phi_{\cdot,1}$) and $Q_r - 1$ zero column vectors with length Q_r , and $\text{diag}(\cdot)$ is the diagonal matrix with diagonal elements $(0, \Phi_{22}, \dots, \Phi_{Q_r Q_r})$. In practice, this means matrix operations can be evaluated using efficient vector-broadcasting, rather than matrix multiplication, routines.

To the best of our knowledge, direct construction of sparse Cholesky factors using explicit expressions as above has not been employed in Gaussian process models. Rather, where constrained covariance forms such as given at (3) are used, including in sparse methods discussed at §2, it is in the context of prediction on test points that are conditionally independent given some inducing set of variables or latent functions [see e.g. 20].

4.2.1 Implicit Sparsity in Exact GP Priors

In some cases construction of a Gram matrix, associated Cholesky factor and inverse using general routines and using (4) - (7) are equivalent. This is due to certain kernels implicitly giving rise to the identity in (6). Where kernels can be expressed as products of real-valued functions of \mathbf{h}_i and \mathbf{h}_j , i.e. assuming $\kappa(\mathbf{h}_i, \mathbf{h}_j) = \phi(\mathbf{h}_i)\psi(\mathbf{h}_j)$, and assuming the inverses $(\phi(\mathbf{h}_i)^{-1}, \psi(\mathbf{h}_j)^{-1})$ are defined for all $\mathbf{h}_i, \mathbf{h}_j \in \mathbf{H}$, kernels give rise to this identity (see the supplement for details). The requirement for symmetry in Mercer kernels [see, e.g. 15] requires $\kappa(\mathbf{h}_i, \mathbf{h}_j) = \kappa(\mathbf{h}_j, \mathbf{h}_i)$, implying $g(\mathbf{h}_i)h(\mathbf{h}_j) = g(\mathbf{h}_j)h(\mathbf{h}_i)$ for all $\mathbf{h}_i, \mathbf{h}_j \in \mathbf{H}$.

In a univariate GP where $\phi(\mathbf{h})$ and $\psi(\mathbf{h})$ are identical, this kernel form is a particular case of the Relevance Vector Machine of Tipping [29]. However, we note that functions $(\phi(\mathbf{h}), \psi(\mathbf{h}))$ need not be identical for (6) to hold.

Trivially, multiplicative kernels comprised of kernel functions that have the property at (6) retain this property. Thus Gram matrices that can be expressed as the Hadamard product of matrices constructed via kernel functions of this type also retain the properties at (4).

Kernels that meet this criterion include constant kernels, polynomial kernels in one dimension, dot product wavelet kernels, and separable stationary kernels (see [15]). All

these kernels decompose multiplicatively into real valued functions of inputs points \mathbf{h}_i and \mathbf{h}_j in a straightforward way. Other, as yet unidentified, kernels may also give rise to the identity in (6).

4.2.2 Properties of Implicitly Sparse Kernels

Direct decomposition: When kernels decompose multiplicatively for any points \mathbf{h}_i , \mathbf{h}_j and \mathbf{h}_k , the Cholesky has the form defined by (7). The Cholesky can be expressed and directly constructed in this way because the relationship holds for any three points. Therefore *any point can be assigned as the ‘pivot’ point κ_{11} and pairwise covariances between any other two points can be expressed in terms of covariances with κ_{11} .*

Degeneracy: A corollary of this, however, is that where (6) holds, only one point on the diagonal is nonzero, Φ_{11} , since for all other points, $\kappa_{ii} - \kappa_{i1}\kappa_{11}^{-1}\kappa_{1i} = 0$ (from (7)). This implies the Cholesky factor consists of a single nonzero column and \mathbf{K} is singular. This in turn implies that the GP is degenerate.¹ The kernels listed above that decompose multiplicatively are positive semi-definite, as opposed to strictly positive definite, Mercer kernels [22, 37]. One of the key criticisms of the degenerate model is that, where kernels are distance-based, predictive variance has the undesirable property of reducing with distance from observed points. In the limit, variance of predictions at new points can be zero [19].

Avoiding degeneracy in GGP models: Issues around degeneracy are avoided in our framework for two reasons. First, use of a sparse construction is limited to \mathbf{K}_{hh}^r . In essence, the model induces sparsity over *tasks* rather than *observations*. Under multi-task latent function mixing approaches, including GGP, it is generally the case that predictions are not being made on new tasks. As such, there is no degeneration over test points since (notional) locations across latent functions are fixed for both training and test observations.

Secondly, as is common practise we add a Kronecker delta kernel (see [15]) to diagonal elements, however excluding the pivot which maintains the model as an exact GP prior without losing the direct Cholesky construction. This is possible because, for \mathbf{K}_{hh}^r , the pivot function input point is known and does not change. The choice of pivot is discussed at §6.

¹The latter follows from the result provided in [21] that a GP is degenerate iff the covariance function has a finite number of nonzero eigenvalues.

5 INFERENCE

Inference for the sparse GGP follows the sparse variational approach of [10] where the prior at (1) is augmented with inducing variables $\{\mathbf{u}_r\}_{r=1}^R$, drawn from the same GP priors as \mathbf{F}_r at M inducing points \mathbf{Z}_r in the same space as \mathbf{X} , giving

$$p(\mathbf{u}|\boldsymbol{\theta}) = \prod_{r=1}^R \mathcal{N}(\mathbf{u}_r; \mathbf{0}, \mathbf{K}_{uu}^r), \text{ and} \quad (8)$$

$$p(\mathbf{F}|\mathbf{u}) = \prod_{r=1}^R \mathcal{N}(\mathbf{F}_r; \tilde{\boldsymbol{\mu}}_r, \tilde{\mathbf{K}}_r), \quad (9)$$

where $\tilde{\boldsymbol{\mu}}_r = \mathbf{A}_r \mathbf{u}_r$, $\tilde{\mathbf{K}}_r = \mathbf{K}_{ff}^r - \mathbf{A}_r \mathbf{K}_{uf}^r$ and $\mathbf{A}_r = \mathbf{K}_{fu}^r (\mathbf{K}_{uu}^r)^{-1} = \mathbf{I}_{Q_r} \otimes \mathbf{K}_{zz}^r (\mathbf{K}_{zz}^r)^{-1}$. $\mathbf{K}_{uu}^r \in \mathbb{R}^{M_{Q_r} \times M_{Q_r}}$ is governed by $\kappa_r(f_j(\mathbf{x}), f_{j'}(\mathbf{x}'))$ evaluated over $\mathbf{Z}_r, \mathbf{H}_r$, similarly yielding the decomposition $\mathbf{K}_{uu}^r = \mathbf{K}_{hh}^r \otimes \mathbf{K}_{zz}^r$. The joint posterior distribution over $\{\mathbf{F}, \mathbf{u}\}$ is approximated by variational inference with

$$p(\mathbf{F}, \mathbf{u}|\mathbf{Y}) \approx q(\mathbf{F}, \mathbf{u}|\boldsymbol{\lambda}) \stackrel{\text{def}}{=} p(\mathbf{F}|\mathbf{u})q(\mathbf{u}|\boldsymbol{\lambda})$$

where the general form of $q(\mathbf{u}|\boldsymbol{\lambda})$ is a mixture of Gaussians as in [10, 11],

$$q(\mathbf{u}|\boldsymbol{\lambda}) = \sum_{k=1}^K \pi_k \prod_{r=1}^r q_k(\mathbf{u}_r|\boldsymbol{\lambda}_{kr}) \quad (10)$$

where $q_k(\mathbf{u}_r|\boldsymbol{\lambda}_{kr}) = \mathcal{N}(\mathbf{u}_r; \mathbf{m}_{kr}, \mathbf{S}_{kr})$ and $\boldsymbol{\lambda}_{kr} = \{\mathbf{m}_{kr}, \mathbf{S}_{kr}, \pi_k\}$.

Prediction for a new point \mathbf{y}_* given \mathbf{x}_* is taken as the expectation over the general posterior distribution for the new point:

$$p(\mathbf{y}_*|\mathbf{x}_*) = \sum_{k=1}^K \pi_k \int p(\mathbf{y}_*|\mathbf{f}_*) q_k(\mathbf{f}_*|\boldsymbol{\lambda}_k) d\mathbf{F}_*, \quad (11)$$

where $q_k(\mathbf{f}_*|\boldsymbol{\lambda}_k)$ is defined as for $q_{k(n)}(\mathbf{f}_{(n)}|\boldsymbol{\lambda}_k)$ below (see §5.2). The expectation in Eq. (11) is estimated by sampling: $\mathbb{E}_{p(\mathbf{y}_*|\mathbf{x}_*)}[\mathbf{y}_*] \approx \frac{1}{S} \sum_{s=1}^S \mathbf{W}_*^s \mathbf{g}_*^s$, where $\{\mathbf{W}_*^s, \mathbf{g}_*^s\} = \mathbf{f}_*^s$ are samples from $q_k(\mathbf{f}_*|\boldsymbol{\lambda}_k)$.

We optimize the evidence lower bound (ELBO) defined as $\mathcal{L}_{\text{elbo}} \stackrel{\text{def}}{=} \mathcal{L}_{\text{ent}} + \mathcal{L}_{\text{cross}} + \mathcal{L}_{\text{ell}}$ where \mathcal{L}_{ent} , $\mathcal{L}_{\text{cross}}$ and \mathcal{L}_{ell} are entropy, cross entropy and expected log likelihood terms, respectively. Derivations of the general expressions for the GP model and ELBO can be found at [10, 11]. In evaluating the efficiency of our approach we consider both a diagonal and Kronecker structure for \mathbf{S}_{kr} . We define the Kronecker specification as $\mathbf{S}_{kr} = \mathbf{S}_{krb} \otimes \mathbf{S}_{krw}$ where $\mathbf{S}_{krb} \in \mathbb{R}^{Q_r \times Q_r}$ and $\mathbf{S}_{krw} \in \mathbb{R}^{M \times M}$ are both sparse, freely parameterized matrices that heuristically correspond to ‘between’ and ‘within’ covariance components. Sparsity is induced via Cholesky factors of the form at (7).

5.1 COMPLEXITY OF LOWER BOUND

We consider complexity of key terms required for inference and prediction for sparse versus non sparse models in the following sections, specifically complexity per group of latent functions. In the discussion that follows, it is assumed that d -dimensioned matrix inverses can be evaluated with complexity $\mathcal{O}(d^3)$ in the general case and $\mathcal{O}(d)$ in sparse or diagonal cases due to nonzero elements of sparse matrices growing linearly with d (see §4.1). It is also assumed that $Q_r \leq M$.

Entropy The entropy component of ELBO is approximated by

$$\mathcal{L}_{\text{ent}} \geq - \sum_{k=1}^K \pi_k \log \sum_{l=1}^K \pi_l \mathcal{N}(\mathbf{m}_k; \mathbf{m}_l, \mathbf{S}_k + \mathbf{S}_l) \quad \text{with}$$

$$\mathcal{N}(\mathbf{m}_k; \mathbf{m}_l, \mathbf{S}_k + \mathbf{S}_l) = \prod_{r=1}^R \mathcal{N}(\mathbf{m}_{kr}; \mathbf{m}_{lr}, \mathbf{S}_{kr} + \mathbf{S}_{lr}). \quad (12)$$

The normal terms in (12) differ in complexity over posterior forms and whether $l = k$. In the case where $K > 1$ and with a Kronecker posterior, both the general and sparse GGP have poor scalability since evaluation requires the log determinant and inverse of $\mathbf{S}_{kr} + \mathbf{S}_{lr}$ with complexity $\mathcal{O}((MQ_r)^3)$. Hence, we consider $K = 1$ or diagonal posteriors for $K \geq 1$. In the diagonal case time and space complexity is $\mathcal{O}(MQ_r)$ for sparse and non sparse models ($\mathcal{O}(KMQ_r)$ for $K > 1$).

For the non-diagonal case, $l = k \implies \mathbf{m}_k = \mathbf{m}_l$, hence the entropy component for each group r reduces to $-\frac{1}{2}(\log |\mathbf{S}_{kr}|) - C$ where C is constant with respect to model parameters. Since the log determinant decomposes as $\log |\mathbf{S}_{kr}| = Q_r M \ln 2 + M \ln |\mathbf{S}_{krb}| + Q_r \ln |\mathbf{S}_{krw}|$ evaluation depends only on the diagonal with complexity $\mathcal{O}(Q_r + M)$. The cost of storage is $\mathcal{O}(Q_r + M)$ versus $\mathcal{O}(Q_r^2 + M^2)$ for sparse and general cases.

Cross Entropy $\mathcal{L}_{\text{cross}}$ has several components that differ across sparse and general models, since

$$\mathcal{L}_{\text{cross}}(\boldsymbol{\lambda}) = -\frac{1}{2} \sum_{k=1}^K \pi_k \sum_{r=1}^R [M_r \log(2\pi) + \log |\mathbf{K}_{uu}^r| + \mathbf{m}'_{kr} (\mathbf{K}_{uu}^r)^{-1} \mathbf{m}_{kr} + \text{tr}((\mathbf{K}_{uu}^r)^{-1} \mathbf{S}_{kr})]$$

Evaluation of $\mathcal{L}_{\text{cross}}$ involves three potentially costly expressions, $|\mathbf{K}_{uu}^r|$, $(\mathbf{K}_{uu}^r)^{-1} \mathbf{m}_{kr}$ and $\text{tr}((\mathbf{K}_{uu}^r)^{-1} \mathbf{S}_{kr})$, naively $\mathcal{O}((MQ_r)^3)$, considered in turn below.

Log determinant: Similar to the entropy term, the expression $|\mathbf{K}_{uu}^r|$ decomposes to require only the calcula-

tion of $|\mathbf{K}_{hh}^r|$ and $|\mathbf{K}_{zz}^r|$ in $\mathcal{O}(M^3 + Q_r^3)$ or $\mathcal{O}(M^3 + Q_r)$ per group for general and sparse models respectively.

Matrix-vector term: The winged diagonal form of $(\mathbf{K}_{hh}^r)^{-1}$ enables computation of $(\mathbf{K}_{uu}^r)^{-1} \mathbf{m}_{kr}$ in $\mathcal{O}(M^3 + Q_r^3)$ time in the general case and $\mathcal{O}(M^3 + Q_r)$ in the sparse case.

Trace term: The trace term involves both prior and posterior covariance matrices. For the Kronecker posterior which allows $\text{tr}((\mathbf{K}_{uu}^r)^{-1} \mathbf{S}_{kr}) = \text{tr}((\mathbf{K}_{hh}^r)^{-1} \mathbf{S}_{krb}) \text{tr}((\mathbf{K}_{zz}^r)^{-1} \mathbf{S}_{krw})$ complexity is reduced from $\mathcal{O}(M^3 + Q_r^3)$ to $\mathcal{O}(Q_r) + \mathcal{O}(M^3)$ from the general to sparse. Where \mathbf{S}_{kr} is diagonal, the trace term requires only diagonal elements of $(\mathbf{K}_{hh}^r)^{-1}$, $(\mathbf{K}_{zz}^r)^{-1}$ and \mathbf{S}_{kr} leading to $\mathcal{O}(Q_r + M^3 + MQ_r)$ versus $\mathcal{O}(Q_r^3 + M^3 + MQ_r)$ in the general case.

Expected Log Likelihood \mathcal{L}_{ell} is defined as

$$\mathcal{L}_{\text{ell}}(\boldsymbol{\lambda}) = \sum_{n=1}^N \mathbb{E}_{q_{(n)}(\mathbf{f}_{(n)}|\boldsymbol{\lambda})} [\log p(\mathbf{y}_{(n)}|\mathbf{f}_{(n)}, \boldsymbol{\phi})] \quad (13)$$

where we estimate the expectation in (13) by Monte Carlo sampling from posterior distributions on $\mathbf{f}_{(n)}$, $q_{(n)}(\mathbf{f}_{(n)}|\boldsymbol{\lambda})$, discussed below.

5.2 INDIRECT SAMPLING

Sampling from the posterior distribution of $\mathbf{f}_{(n)}$ and similarly \mathbf{f}_* is required for both \mathcal{L}_{ell} and prediction. [10] show that samples from $q_{(n)}(\mathbf{f}_{(n)}|\boldsymbol{\lambda})$ can be drawn from component group posteriors i.e. $q_{k(n)}(\mathbf{f}_{(n)}|Q_r, \boldsymbol{\lambda}_{kr}) = \mathcal{N}(\mathbf{b}_{kr(n)}, \boldsymbol{\Sigma}_{kr(n)})$ with mean and covariance expressions given by $\mathbf{b}_{kr(n)} = \mathbf{A}_{r(n)} \mathbf{m}_{kr}$ and $\boldsymbol{\Sigma}_{kr(n)} = \tilde{\mathbf{K}}_{r(n)} + \mathbf{A}_{r(n)} \mathbf{S}_{kr} \mathbf{A}_{r(n)}'$, where $\tilde{\mathbf{K}}_{r(n)}$ and $\mathbf{A}_{r(n)} \mathbf{S}_{kr} \mathbf{A}_{r(n)}'$ are defined as in 8. Detailed expressions are provided in the Supplement.

Direct sampling as in [10] requires factorizing the posterior covariance to obtain a premultiplier $\Psi(\boldsymbol{\Sigma}_{kr(n)})$ such that $\Psi \Psi' = \boldsymbol{\Sigma}_{kr(n)}$. However, since this differs for each observation the associated cost per group is $\mathcal{O}(NQ_r^3)$, where N is mini-batch size for \mathcal{L}_{ell} sampling or N_{test} for prediction. Further, batch factorization is inherently unstable.

We avoid this by making use of known Cholesky factors and sampling from two component distributions using the property that the sum of two independent, normally distributed random variables, $\mathbf{X} \sim \mathcal{N}(\boldsymbol{\mu}_{\mathbf{X}}, \boldsymbol{\Sigma}_{\mathbf{X}})$ and $\mathbf{Y} \sim \mathcal{N}(\boldsymbol{\mu}_{\mathbf{Y}}, \boldsymbol{\Sigma}_{\mathbf{Y}})$ is also a normally distributed with mean $\boldsymbol{\mu}_{\mathbf{X}} + \boldsymbol{\mu}_{\mathbf{Y}}$ and covariance $\boldsymbol{\Sigma}_{\mathbf{X}} + \boldsymbol{\Sigma}_{\mathbf{Y}}$. We draw independent samples from two distributions specified as $\mathcal{N}(\mathbf{0}, \tilde{\mathbf{K}}_{r(n)})$

and $\mathcal{N}(\mathbf{b}_{kr(n)}, \mathbf{A}_{r(n)} \mathbf{S}_{kr} \mathbf{A}_{r(n)}')$, and sum these to return samples from $\mathcal{N}(\mathbf{b}_{kr(n)}, \mathbf{\Sigma}_{kr(n)})$.

Complexity of factorizations for $\tilde{\mathbf{K}}_{r(n)}$ and $\mathbf{A}_{r(n)} \mathbf{S}_{kr} \mathbf{A}_{r(n)}'$ differs across variants but where a sparse prior is adopted, is reduced to $\mathcal{O}(NQ_r)$. Critically, in the sparse case memory complexity is significantly reduced by replacing the premultiplier $\Psi(\tilde{\mathbf{K}}_{r(n)})$ with vector operations reducing memory complexity from $\mathcal{O}(NQ_r^2)$ to $\mathcal{O}(NQ_r)$.

Overall, indirect sampling reduces time, but not memory, complexity relative to direct sampling in the general model. However, by using sparse priors it is possible to achieve significant reductions from the general indirect model. Further gains still are possible if a sparse Kronecker posterior is used in lieu of a diagonal posterior. The last point arises since (broadly speaking) operations involving sparse matrices can exploit decomposition properties of the Kronecker product to achieve linear complexity that is additive, rather than multiplicative, over M and Q_r . The same observation may be made about complexity reductions in entropy and cross entropy terms. Further details are provided in the Supplement.

6 APPLICATION TO SOLAR

We test the sparse GGP model on solar forecasting applications, where tasks are solar sites and the modelling goal is to jointly predict power output at all sites at each test time point n . The sparse GGP model for solar follows the approach in [10] where, for P tasks, there are P latent node functions, meaning $Q_g(P+1) = Q$. Latent weight functions are grouped according to rows of $\mathbf{W}_{(n)}$ while latent node functions are assumed to be independent. Thus, predicted output at site i , $y_{(n)i}$, is a linear combination of (site-associated) node functions. Spatial features, $\mathbf{h}_j = (\text{latitude}_j, \text{longitude}_j)$, $j = 1, \dots, Q_r$, populate the cross function feature matrix \mathbf{H}_r for every group.

For node functions, $\kappa_{\mathbf{g}_j}(\mathbf{x}_t, \mathbf{x}_s)$ is a radial basis function kernel on a vector of lagged power features at site i , i.e. for site i at time t , $\mathbf{l}_{i,t} = (y_{i,t}, y_{i,t-1})$. For each row-group r in $\mathbf{W}_{(n)}$, $\kappa_r(f_j(\mathbf{x}), f_{j'}(\mathbf{x}')) = \kappa_r(\mathbf{x}, \mathbf{x}') \kappa_r(\mathbf{h}_j, \mathbf{h}_{j'})$ with $\kappa_r(\mathbf{x}, \mathbf{x}') = \kappa_{Per.}(t, s) \kappa_{RBF}(\mathbf{l}_{rt}, \mathbf{l}_{rs})$, where $\kappa_{Per.}(t, s)$ is a periodic kernel on a time index t .

6.1 SOLAR MODEL VARIANTS

6.1.1 Selection of Sparsity Constraints *a priori*

Given the spatial nature of covariance between sites and where node functions align with tasks, the weight applied

to each node by a given task would be expected to be a function of the (notional) spatial location of the node relative to the target task. We assume that weights are conditionally independent given the weight assigned to the task-associated node for that node. We enforce this constraint for each row-group i of $\mathbf{W}_{(n)}$,

$$\mathbf{W}_{(n)ij} \perp \mathbf{W}_{(n)ik} \mid \mathbf{W}_{(n)ii} \quad (14)$$

$j, k \neq i, j \neq k$. Since latent function groupings in the GGP framework can be any subset of \mathbf{F} in any order, it is only required that, for sparse inference, latent functions within each group $\mathbf{W}_{(n)i}$ are ordered such that $\mathbf{W}_{(n)ii}$ acts as the pivot. Within each row of weights, this gives rise to the star configuration for the undirected graphical model as illustrated at Figure 1, with a single pivot weight function ($\mathbf{W}_{(n)ii}$), and conditionally independent child weight functions corresponding to cross-site nodes ($\mathbf{W}_{(n)ij}, j \neq i$).

6.1.2 Cross Function Kernel Variants

We test three sparse forms of $\mathbf{K}_{\mathbf{hh}}^T$, which we term (a) ‘implicitly sparse’ (sparsity is automatic i.e. implicit in the model due to separable kernel specification as discussed at §4.2.1), (b) ‘explicitly sparse’ (a stationary kernel that does not give rise to automatic sparsity but is used in conjunction with the constraint in (6) explicitly imposed), and (c) ‘undefined sparsity’ ($\mathbf{K}_{\mathbf{hh}}^T$ is freely parameterized using $2Q_r - 1$ parameters for nonzero Cholesky elements and no kernel form is defined).

In the implicitly sparse case, we use a separable, dot product wavelet kernel with Ricker mother wavelet function (see [37]) plus diagonal correction as described at §4.2.1, which we assume to be shared across groups. The full kernel is given by $\kappa_{r(wav.)} + \kappa_{r(diag)}$ and the (full rank) sparse Cholesky can be constructed as in (7) with $\Phi_{ii} = \sqrt{\kappa_{r(diag)}}, i \neq 1$.

For the explicit sparsity case, we use a combined radial basis, Epanechnikov kernel function with the constraint at (6) enforced by setting $\text{Chol}(\mathbf{K}_{\mathbf{hh}}^r)_{j,k} = 0, j, k \neq 1, j \neq k$. Specifically, $\kappa_r(\mathbf{h}_j, \mathbf{h}_{j'}) = \kappa_{RBF}(\mathbf{h}_j, \mathbf{h}_{j'}) \kappa_{Ep.}(\mathbf{h}_j, \mathbf{h}_{j'}), j, j' = 1 \dots P$.

6.2 EXPERIMENTS

We test our model using two datasets (with $P = 25$ and $P = 50$). For $P = 25$ we evaluate performance relative to the general GGP and two scalable benchmark models. In addition, we test a general GGP model with full, freely parameterized cross site covariance. For $P = 50$, we evaluate sparse models using Kronecker posteriors against non GGP benchmarks however other GGP models could

not be estimated under the same platform constraints. All models use $K = 1$.

Data are five minute average power output between 7am and 7pm. The first dataset consists of 25 proximate sites over 45 days in Spring with 105,000 (57,000) observations for training (testing). The second dataset consists of 50 proximate sites in a different location and season (Autumn) with 210,000 (114,000) observations in total for training (testing).

Two classes of non-GGP benchmark models are considered, the linear coregional model (LCM) and GPRN models. These benchmarks are chosen as they can be implemented in the same inference framework as the GGP and sparse GGP, allowing direct comparison of model performance.² For the LCM model, we report two specifications for $P = 25$. The first mirrors the GGP with $P = Q_g$ and the second is a lower ranked model with $Q_g = 5$ ($Q_g = 4$) for diagonal (Kronecker) posteriors. For $P = 50$ we report only the first specification (the best LCM model based on RMSE). For the GPRN, we report models with $Q_g = 2$. This was the best performing specification for $P = 25$, and the largest value for Q_g able to run on the same platform as sparse GGP models.

For GPRN latent functions in a row \mathbf{W}_i , the kernel is defined as $\kappa_{Per.}(t, s)\kappa_{RBF}(\mathbf{l}_{it}, \mathbf{l}_{is})$. For node functions, we use a radial basis kernel with lag features. For LCM $P = Q_g$, node functions are defined as combined periodic-radial basis kernels. For lower rank mixing models, we tested two node specifications for $Q_g = 2, 3, 4, 5$, (a) lags for all sites assigned to each node function, and (b) subsets of lags assigned to node functions based on k-means clustering of lags into Q_g groups. Reported benchmarks for LCM use clustered lags, while GPRN benchmarks use complete lags per node.

6.2.1 Experimental Settings

All models are estimated based on the variational framework explained in §5 with indirect sampling used for both sparse and general models. Starting values for common components were set to be equal across all models and the number of inducing points per group of latent functions is set to approximately standardize computational complexity per iteration relating to RM^3 , using $M = 200$ per GGP group as the baseline.

The ELBO is iteratively optimized until its relative change over successive epochs is less than 10^{-5} up to a maximum of 200 epochs or maximum of 20 hours. Optimization is performed using ADAM [18] with settings $\{LR = 0.005; \beta_1 = 0.09; \beta_2 = 0.99\}$. All data except

²The multi task model of [6] is not included as prior experiments found the model to be uncompetitive for this problem.

time index features are normalized prior to optimization. Time and performance measures are captured every five epochs. Timed experimental results reported exclude time required to compute and store the various performance measures during optimization. All models are estimated on a multi-GPU machine with four NVIDIA TITAN Xp graphics cards (memory per card 12GB; clock rate 1.58 GHz). Experiments were run until either convergence criteria were reached, or to a maximum of 200 epochs or 1200 minutes runtime.

6.2.2 Results

Results for all models are reported at Table 1 with further details available in the Supplement. For $P = 25$ forecast accuracy of sparse and general GGP models is comparable. Results for sparse and non sparse GGP models differ by only 1 to 3 percent (respectively) over the best performing models on RMSE and MAE, while NLPD results are slightly more variable. Differences between diagonal and Kronecker posteriors are also fine, with neither model showing clear advantage on accuracy although we note that forecast variance is slightly improved under Kronecker posteriors. For $P = 25$, accuracy is comparable for GGP and GPRN on MAE and RMSE, however GGP based models perform significantly better than benchmarks on NLPD. The LCM performs relatively poorly on all measures. Mean forecast variance was also found to be significantly lower under GGP models. For $P = 50$, sparse GGP models outperform benchmark models on all accuracy and variance measures.

Model efficiency Average time cost (as captured every fifth epoch) of mini batch step time, full ELBO computation time and prediction computation time for the full test set is shown at Figure 2 for sparse versus general GGP models. Results confirm that sparse GGP models have lower time costs than general counterparts; step time and ELBO computation time are decreased by 10 to 19 percent and 11 to 21 percent respectively. We observe that the theoretical reduction in complexity is not fully realized in our experiments. We attribute this to the lack of sparsity support for some of the operations in our environment, specifically instantiations of the sparse inverse in the cross entropy trace and matrix-vector terms.

The most substantial improvements, however, are for prediction, where sparse models are three to four times faster over the full test set. Further, mean sparse model prediction time scales approximately linearly between $P = 25$ (at 3.5 seconds) and $P = 50$ (at 9 seconds).

We also find that, for the same prior, average time cost is always lower under the Kronecker posterior, consistent with their lower complexity as discussed in 5. Further,

Table 1: Forecast Accuracy of GGP, Sparse GGP and Benchmark Models. Results shown for diagonal (diag) and Kronecker (Kron) posteriors with $K = 1$ for Adelaide ($P = 25$) and Sydney ($P = 50$) datasets. Results are reported for best performing GPRN and LCM benchmarks (based on RMSE) and for LCM where $Q_g = P$.

| $P = 25$ | | RMSE | MAE | NLPD |
|-----------------------|--------|--------------|--------------|--------------|
| GGP | (diag) | 0.343 | 0.216 | 0.399 |
| GGP (free) | (diag) | 0.345 | 0.215 | 0.378 |
| Sparse GGP (implicit) | (diag) | 0.342 | 0.215 | 0.412 |
| Sparse GGP (explicit) | (diag) | 0.345 | 0.216 | 0.381 |
| Sparse GGP (free) | (diag) | 0.346 | 0.218 | 0.380 |
| LCM ($Q_g = P$) | (diag) | 0.371 | 0.235 | 0.553 |
| LCM ($Q_g = 5$) | (diag) | 0.366 | 0.239 | 0.481 |
| GPRN ($Q_g = 2$) | (diag) | 0.344 | 0.217 | 0.451 |
| <hr/> | | | | |
| GGP | (Kron) | 0.343 | 0.213 | 0.382 |
| GGP (free) | (Kron) | 0.344 | 0.213 | 0.384 |
| Sparse GGP (implicit) | (Kron) | 0.345 | 0.217 | 0.419 |
| Sparse GGP (explicit) | (Kron) | 0.342 | 0.212 | 0.375 |
| Sparse GGP (free) | (Kron) | 0.346 | 0.214 | 0.385 |
| LCM ($Q_g = P$) | (Kron) | 0.375 | 0.236 | 0.583 |
| LCM ($Q_g = 4$) | (Kron) | 0.367 | 0.240 | 0.475 |
| GPRN ($Q_g = 2$) | (Kron) | 0.342 | 0.214 | 0.446 |
| <hr/> | | | | |
| $P = 50$ | | RMSE | MAE | NLPD |
| Sparse GGP (implicit) | (Kron) | 0.423 | 0.256 | 0.639 |
| Sparse GGP (explicit) | (Kron) | 0.420 | 0.258 | 0.611 |
| Sparse GGP (free) | (Kron) | 0.425 | 0.260 | 0.636 |
| LCM ($Q_g = P$) | (Kron) | 0.451 | 0.283 | 0.807 |
| GPRN ($Q_g = 2$) | (Kron) | 0.428 | 0.263 | 0.664 |

freely parameterized GGP models have lower time costs than ‘standard’ counterparts reflecting the lower complexity of operations on \mathbf{K}_{hh}^r elements where the model is freely parameterized ($\mathcal{O}(1)$ versus $\mathcal{O}(H)$ for featurized kernels). Time costs for benchmark models are significantly lower than sparse GGP based models, in the order of four to ten times faster per operation (see the Supplement for details).

7 DISCUSSION

We have shown that by exploiting known properties of multivariate Gaussians and conditional independence across latent functions, it is possible to significantly improve the scalability of multi task mixing models with respect to the number of functions. We have applied this approach to the problem of solar forecasting at multiple distributed sites using two large multi task datasets and demonstrated that both spatially driven and freely parameterized sparse cross function covariance structures can be exploited to achieve faster learning and prediction without

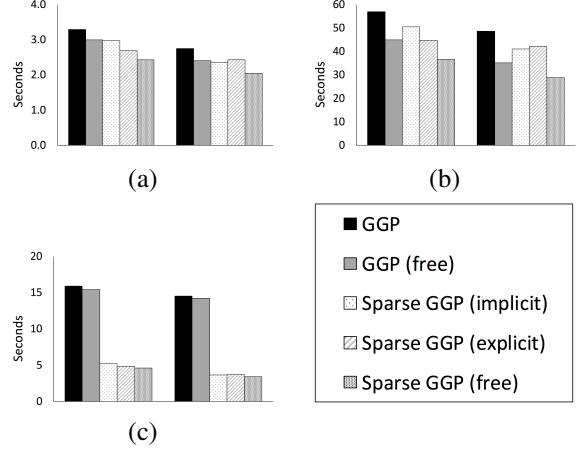


Figure 2: Computation Times for GGP Versus Sparse GGP Models ($P = 25$). Panel (a) shows average time for a single minibatch step. Panel (b) shows average time to compute the full evidence lower bound. Panel (c) shows average time to compute predictions over the full test set. Results for diagonal (Kronecker) posteriors are shown in left (right) group for each panel.

sacrificing forecast performance. In particular the cost of prediction is dramatically reduced and shown to be linear in the number of grouped latent functions.

We focus our efforts on efficient structures for cross site covariance, however we note that this is not incompatible with further efficiencies that might be considered to reduce complexity on the number of inducing points, including sparse covariance, structured inputs and low rank approximations. The approach can be seen as an avenue to extend sparse models to multi task mixing frameworks.

Acknowledgments

This research was conducted with support from the Co-operative Research Centre for Low-Carbon Living in collaboration with the University of New South Wales and Solar Analytics Pty Ltd.

A SUPPLEMENTARY MATERIAL

A.1 Expressions for multivariate Gaussian precision matrix

The precision matrix from [26, 32], has a sparse, winged diagonal form

$$\mathbf{\Lambda} = \begin{bmatrix} \mathbf{\Lambda}_{11} & \mathbf{\Lambda}'_{21} & \mathbf{\Lambda}'_{31} & \cdots & \mathbf{\Lambda}'_{Q_r,1} \\ \mathbf{\Lambda}_{21} & \mathbf{\Lambda}_{22} & 0 & \cdots & 0 \\ \mathbf{\Lambda}_{31} & 0 & \mathbf{\Lambda}_{33} & \cdots & 0 \\ \vdots & \vdots & \vdots & \ddots & \vdots \\ \mathbf{\Lambda}_{Q_r,1} & 0 & 0 & \cdots & \mathbf{\Lambda}_{Q_r,Q_r} \end{bmatrix}$$

where

$$\begin{aligned} \mathbf{\Lambda}_{11} &= \mathbf{K}_{11}^{-1} + \sum_{i=2}^{Q_r} \mathbf{K}_{11}^{-1} \mathbf{K}_{1i} \mathbf{K}_{ii,1}^{-1} \mathbf{K}_{i1} \mathbf{K}_{11}^{-1} \\ \mathbf{\Lambda}_{i1} &= -\mathbf{K}_{11}^{-1} \mathbf{K}_{1i} \mathbf{K}_{ii,1}^{-1} \\ \mathbf{\Lambda}_{ii} &= \mathbf{K}_{ii,1}^{-1}, \quad \text{where} \\ \mathbf{K}_{ii,1}^{-1} &= \mathbf{K}_{ii} - \mathbf{K}_{i1} \mathbf{K}_{11}^{-1} \mathbf{K}_{1i}, \quad i = 2, \dots, Q_r \end{aligned}$$

The sparse Cholesky factor of \mathbf{K} has the form

$$\mathbf{\Phi} = \begin{bmatrix} \mathbf{\Phi}_{11} & 0 & 0 & \cdots & 0 \\ \mathbf{\Phi}_{21} & \mathbf{\Phi}_{22} & 0 & \cdots & 0 \\ \mathbf{\Phi}_{31} & 0 & \mathbf{\Phi}_{33} & \cdots & 0 \\ \vdots & \vdots & \vdots & \ddots & \vdots \\ \mathbf{\Phi}_{Q_r,1} & 0 & 0 & \cdots & \mathbf{\Phi}_{Q_r,Q_r} \end{bmatrix}$$

where

$$\begin{aligned} \mathbf{\Phi}_{11} &= \text{Chol}(\kappa_{11}), \quad \mathbf{\Phi}_{i1} = \kappa_{i1}(\mathbf{\Phi}_{11})^{-1}, \quad \text{and} \\ \mathbf{\Phi}_{ii} &= \text{Chol}(\kappa_{ii} - \kappa_{i1} \kappa_{11}^{-1} \kappa_{1i}). \end{aligned}$$

A.2 Proof of implicit sparsity in exact GP priors

Construction of a Gram matrix, associated Cholesky factor and inverse using general routines and direct sparse constructions are equivalent where kernels implicitly give rise to the identity where

$$\begin{aligned} \kappa(\mathbf{h}_i, \mathbf{h}_j) &= \kappa(\mathbf{h}_i, \mathbf{h}_k) \kappa(\mathbf{h}_k, \mathbf{h}_j)^{-1} \kappa(\mathbf{h}_k, \mathbf{h}_j) \\ \iff f(\mathbf{h}_i) \perp f(\mathbf{h}_j) \quad | \quad f(\mathbf{h}_k) \end{aligned} \quad (15)$$

for any points $\mathbf{h}_i, \mathbf{h}_j$ and \mathbf{h}_k .

Where kernels can be expressed as products of real-valued functions of \mathbf{h}_i and \mathbf{h}_j , i.e. assuming $\kappa(\mathbf{h}_i, \mathbf{h}_j) = \phi(\mathbf{h}_i) \psi(\mathbf{h}_j)$, and assuming the inverses $(\phi(\mathbf{h}_i)^{-1}, \psi(\mathbf{h}_j)^{-1})$ are defined for all $\mathbf{h}_i, \mathbf{h}_j \in \mathbf{H}$, kernels give

rise to this identity. To see this, consider a positive semi-definite kernel such that

$$\begin{aligned} \kappa(\mathbf{h}_i, \mathbf{h}_j) &= g(\mathbf{h}_i) h(\mathbf{h}_j) \\ \implies \kappa(\mathbf{h}_k, \mathbf{h}_k)^{-1} &= g(\mathbf{h}_k)^{-1} h(\mathbf{h}_k)^{-1} \\ \implies \kappa(\mathbf{h}_i, \mathbf{h}_j) &= g(\mathbf{h}_i) h(\mathbf{h}_k) g(\mathbf{h}_k)^{-1} h(\mathbf{h}_k)^{-1} \\ &\quad \times g(\mathbf{h}_k) h(\mathbf{h}_j) \\ &= \kappa(\mathbf{h}_i, \mathbf{h}_k) \kappa(\mathbf{h}_k, \mathbf{h}_k)^{-1} \kappa(\mathbf{h}_k, \mathbf{h}_j) \end{aligned} \quad (16)$$

Kernels of this form are valid, positive semi-definite kernels so long as the properties of symmetry and positive semi-definiteness are satisfied. Symmetry implies $\kappa(\mathbf{h}_i, \mathbf{h}_j) = \kappa(\mathbf{h}_j, \mathbf{h}_i)$, implying $g(\mathbf{h}_i) h(\mathbf{h}_j) = g(\mathbf{h}_j) h(\mathbf{h}_i)$ for all $\mathbf{h}_i, \mathbf{h}_j \in \mathbf{H}$. Positive semi-definiteness implies for any examples $\mathbf{h}_i, \mathbf{h}_j$ and any set of real numbers $\lambda_1, \dots, \lambda_l$, $\sum_{i=1}^l \sum_{j=1}^l \lambda_i \lambda_j \kappa(\mathbf{h}_i, \mathbf{h}_j) \geq 0$ [see, e.g. 15].

We note that following diagonal correction the implicitly sparse model is no longer invariant to pivot choice, however is still an exact GP when used as in our model (i.e. to characterize cross function covariance in the mixing model). For a collection of random variables to meet the definition of a GP, it is only required that any finite subset of the collection is jointly Gaussian distributed, not precluding finite index sets [22]. This observation also extends to the explicitly sparse case and undefined, freely parameterized case.

A.3 Complexities for Indirect Sampling

Sampling from the posterior distribution of $\mathbf{f}_{(n)}$ and similarly \mathbf{f}_* is required for both \mathcal{L}_{ell} and prediction. [10] show that samples from $q_{(n)}(\mathbf{f}_{(n)} | \boldsymbol{\lambda})$ can be drawn from component group posteriors i.e. $q_{k(n)}(\mathbf{f}_{(n)Q_r} | \boldsymbol{\lambda}_{kr}) = \mathcal{N}(\mathbf{b}_{kr(n)}, \boldsymbol{\Sigma}_{kr(n)})$ with mean and covariance expressions given by $\mathbf{b}_{kr(n)} = \mathbf{A}_{r(n)} \mathbf{m}_{kr}$ and $\boldsymbol{\Sigma}_{kr(n)} = \tilde{\mathbf{K}}_{r(n)} + \mathbf{A}_{r(n)} \mathbf{S}_{kr} \mathbf{A}'_{r(n)}$, where

$$\begin{aligned} \tilde{\mathbf{K}}_{r(n)} &= \mathbf{K}_{\mathbf{h}\mathbf{h}}^r \times [\kappa_r(\mathbf{x}_{(n)}, \mathbf{x}_{(n)}) \\ &\quad - \kappa_r(\mathbf{x}_{(n)}, \mathbf{Z}_r) (\mathbf{K}_{\mathbf{z}\mathbf{z}}^r)^{-1} \kappa_r(\mathbf{Z}_r, \mathbf{x}_{(n)})] \quad \text{and} \\ \mathbf{A}_{r(n)} &= [\mathbf{I}_{Q_r} \otimes \kappa_r(\mathbf{x}_{(n)}, \mathbf{Z}_r) (\mathbf{K}_{\mathbf{z}\mathbf{z}}^r)^{-1}] \end{aligned}$$

Given a Kronecker posterior the quadratic term simplifies to

$$\begin{aligned} \mathbf{A}_{r(n)} \mathbf{S}_{kr} \mathbf{A}'_{r(n)} &= [\mathbf{S}_{krb} \otimes \\ &\quad \kappa_r(\mathbf{x}_{(n)}, \mathbf{Z}_r) (\mathbf{K}_{\mathbf{z}\mathbf{z}}^r)^{-1} \mathbf{S}_{krw} (\mathbf{K}_{\mathbf{z}\mathbf{z}}^r)^{-1} \kappa_r(\mathbf{Z}_r, \mathbf{x}_{(n)})] \end{aligned}$$

The time costs to factorize the quadratic term $\mathbf{A}_{r(n)} \mathbf{S}_{kr} \mathbf{A}'_{r(n)}$ are $\mathcal{O}(NM^2Q_r + M^3)$, $\mathcal{O}(N(M^2 + Q_r^2) + M^3)$ and $\mathcal{O}(N(M^2 + Q_r) + M^3)$ for the diagonal, general Kronecker and sparse Kronecker posteriors

respectively. Similarly, the time costs of obtaining $\tilde{\mathbf{K}}_{r(n)}$ are $\mathcal{O}(N(M^2 + Q_r^2) + M^3)$ or $\mathcal{O}(N(M^2 + Q_r) + M^3)$ for the general and sparse priors respectively. Direct sampling also requires combination and factorization of these components in $\mathcal{O}(NQ_r^3)$ time and with $\mathcal{O}(NQ_r^2)$ memory.

Indirect sampling requires factorization of $\tilde{\mathbf{K}}_{r(n)}$ in $\mathcal{O}(NQ_r^2 + Q_r^3)$ time for general priors and $\mathcal{O}(NQ_r)$ for sparse priors. Similarly, given a Kronecker posterior, Cholesky factors can be obtained in $\mathcal{O}(NQ_r^2 + Q_r^3)$ and $\mathcal{O}(NQ_r)$ for general and sparse specifications respectively. The cost of $\text{Chol}(\mathbf{A}_{r(n)}\mathbf{S}_{kr}\mathbf{A}'_{r(n)})$ is $\mathcal{O}(NQ_r)$ in the diagonal case.

In the sparse case memory complexity is reduced by replacing the premultiplier $\Psi(\tilde{\mathbf{K}}_{r(n)})$ (and additionally $\Psi(\mathbf{A}_{r(n)}\mathbf{S}_{kr}\mathbf{A}'_{r(n)})$ for Kronecker posteriors) by vector operations such that the premultipliers in $\mathcal{O}(NQ_r^2)$ space are never instantiated. Storage of vector components is reduced to $\mathcal{O}(NQ_r)$ in line with the diagonal premultiplier.

A.4 Additional Experimental Results

Representative results for forecast accuracy over estimation time for RMSE with sparse posterior are shown at Figures 3 and 4. Optimization of benchmark models is significantly faster than GGP based models, however we also find that performance of GGP models on RMSE surpasses that of benchmark models before their optimization is complete for Kronecker posterior models (for NLPD and diagonal posteriors, performance of GGP models improves more gradually but still within reasonable time).

We found rankings in terms of speed at which gains are achieved to be very consistent across accuracy measures and posterior specifications. In particular, LCM and GPRN achieve their gains quickly, followed by explicitly sparse and free sparse GGP models, while general GGP models and implicitly sparse GGP models achieve gains more gradually.

Estimated covariance Illustrative examples of \mathbf{K}_{hh}^r estimated under the different GGP specifications with diagonal posteriors are presented at Figure 5. Heatmaps are shown for different row groups for sites in longitudinal order. As shown for the initial full GGP specification, parameters across row groups were found to be largely consistent with few exceptions (this was also true for latitudinal lengthscales). In contrast, parameters under sparse (explicit) and sparse (implicit) were found to be very adaptive, varying in lengthscale and magnitude. While the explicit sparse construction forces the model to place the most weight on nearest sites, weight centred under the

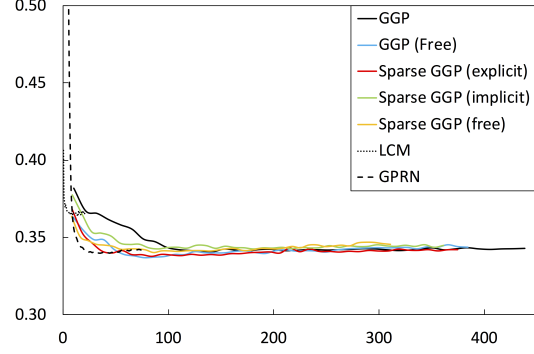


Figure 3: RMSE over optimization time for $P = 25$ with Kronecker posterior.

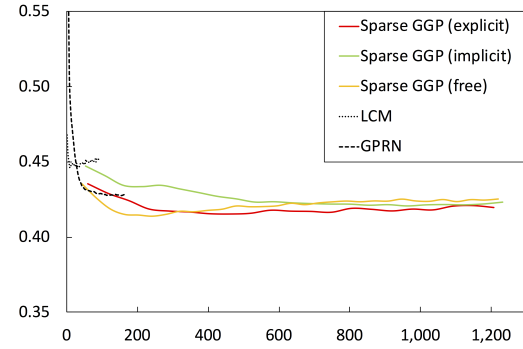


Figure 4: RMSE over optimization time for $P = 50$ with Kronecker posterior.

wavelet kernel broadly tended to nearby sites but far less rigidly. The more constrained covariance structure of the explicit sparse GGP, however, yielded better model performance overall. Freely parameterized models (not shown) did not tend toward covariance structures estimated for models with explicit kernel definitions. Rather, \mathbf{K}_{hh}^r in both the full and sparse free models tended to a very sparse diagonal structure.

Forecast variance In addition to forecast accuracy, model forecast variance and model average rank results are reported at Table 2. Forecast variance is comparable under sparse and non sparse specifications, and in fact is (very) slightly improved under the sparse specifications on average. Results for LCM and GPRN show poorer forecast variance, a disadvantage in energy applications in particular. These findings are consistent with the results of [10], where general GGP models were found to reduce variance relative to benchmark models.

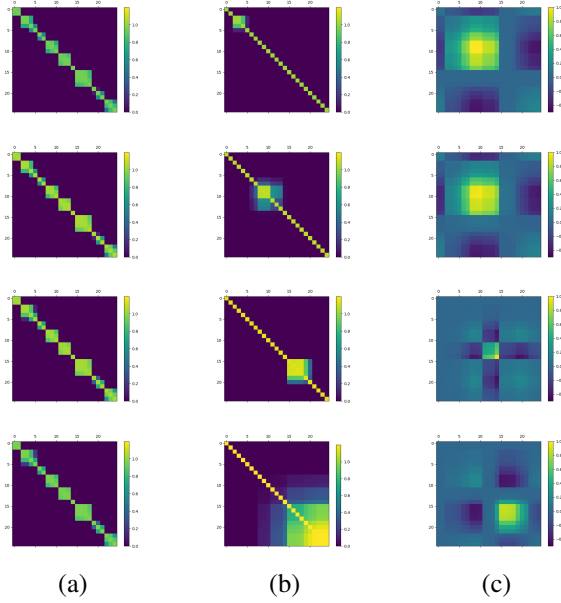


Figure 5: Examples of \mathbf{K}_{hh}^r under GGP and sparse GGP model variants for $P = 25$ (diagonal). Heatmaps of \mathbf{K}_{hh}^r are shown for four row-groups in \mathbf{W} for tasks $i = 2, 10, 18, 24$ for tasks (sites) ordered by site longitude. Estimated \mathbf{K}_{hh}^r shown for GGP (Panel (a)), Sparse GGP (explicit) (Panel (b)) and Sparse GGP (implicit) (Panel (c)). Heatmaps in Panel (c) are shown without the diagonal correction term.

Table 2: Forecast accuracy and variance of GGP, sparse GGP and benchmark models. Results shown for *Diagonal* and *Kronecker* posterior covariances with $K = 1$ for Adelaide ($P = 25$) and Sydney ($P = 50$) datasets. Benchmark results are reported for best performing GPRN and LCM specifications based on RMSE. Results for LCM where $Q_g = P$ are also reported. F-VAR refers to mean prediction variance. M-RANK is defined as average model performance ranking over accuracy measures (RMSE, MAE and NLPD).

| P = 25 | | | | | |
|-----------------------|--------------|--------------|--------------|------------|--------------|
| | RMSE | MAE | NLPD | M-RANK | F-VAR |
| <i>Diagonal</i> | | | | | |
| GGP | 0.343 | 0.216 | 0.399 | 7.3 | 0.121 |
| GGP (free) | 0.345 | 0.215 | 0.378 | 5.7 | 0.116 |
| Sparse GGP (implicit) | 0.342 | 0.215 | 0.412 | 5.3 | 0.127 |
| Sparse GGP (explicit) | 0.345 | 0.216 | 0.381 | 6.0 | 0.117 |
| Sparse GGP (free) | 0.346 | 0.218 | 0.380 | 7.7 | 0.118 |
| LCM ($Q_g = P$) | 0.371 | 0.235 | 0.553 | 12.7 | 0.181 |
| LCM ($Q_g = 5$) | 0.366 | 0.239 | 0.481 | 12.0 | 0.151 |
| GPRN ($Q_g = 2$) | 0.344 | 0.217 | 0.451 | 8.7 | 0.149 |
| <i>Kronecker</i> | | | | | |
| GGP | 0.343 | 0.213 | 0.382 | 4.0 | 0.117 |
| GGP (free) | 0.344 | 0.213 | 0.384 | 4.7 | 0.112 |
| Sparse GGP (implicit) | 0.345 | 0.217 | 0.419 | 8.0 | 0.121 |
| Sparse GGP (explicit) | 0.342 | 0.212 | 0.375 | 1.7 | 0.116 |
| Sparse GGP (free) | 0.346 | 0.214 | 0.385 | 6.7 | 0.111 |
| LCM ($Q_g = P$) | 0.375 | 0.236 | 0.583 | 11.3 | 0.180 |
| LCM ($Q_g = 4$) | 0.367 | 0.240 | 0.475 | 9.7 | 0.147 |
| GPRN ($Q_g = 2$) | 0.342 | 0.214 | 0.446 | 4.7 | 0.150 |
| P = 50 | | | | | |
| | RMSE | MAE | NLPD | M-RANK | F-VAR |
| <i>Kronecker</i> | | | | | |
| Sparse GGP (implicit) | 0.423 | 0.256 | 0.639 | 2.0 | 0.162 |
| Sparse GGP (explicit) | 0.420 | 0.258 | 0.611 | 1.0 | 0.144 |
| Sparse GGP (free) | 0.425 | 0.260 | 0.636 | 2.0 | 0.136 |
| LCM ($Q_g = P$) | 0.451 | 0.283 | 0.807 | 4.0 | 0.211 |
| GPRN ($Q_g = 2$) | 0.428 | 0.263 | 0.664 | 3.0 | 0.185 |

References

- [1] Álvarez, M. and Lawrence, N. D. (2009). Sparse convolved Gaussian processes for multi-output regression. In *Neural Information Processing Systems*.
- [2] Álvarez, M. A. and Lawrence, N. D. (2011). Computationally efficient convolved multiple output Gaussian processes. *Journal of Machine Learning Research*, 12(5):1459–1500.
- [3] Álvarez, M. A., Rosasco, L., and Lawrence, N. D. (2012). Kernels for vector-valued functions: A review. *Found. Trends Mach. Learn.*, 4(3):195–266.
- [4] Antonanzas, J., Osorio, N., Escobar, R., Urraca, R., de Pison, F. M., and Antonanzas-Torres, F. (2016). Review of photovoltaic power forecasting. *Solar Energy*, 136:78 – 111.
- [5] Bonilla, E. V., Agakov, F. V., and Williams, C. K. (2007). Kernel multi-task learning using task-specific features. In *AISTATS*, pages 43–50.
- [6] Bonilla, E. V., Chai, K. M. A., and Williams, C. K. I. (2008). Multi-task Gaussian process prediction. In *Neural Information Processing Systems*.
- [7] Cressie, N. and Wikle, C. K. (2011). *Statistics for spatio-temporal data*. John Wiley & Sons.
- [8] Cutajar, K., Bonilla, E. V., Michiardi, P., and Filippone, M. (2016a). Practical learning of deep Gaussian processes via random fourier features. *ArXiv*, (1610.04386).
- [9] Cutajar, K., Osborne, M., Cunningham, J., and Filippone, M. (2016b). Preconditioning kernel matrices. In *International Conference on Machine Learning*, pages 2529–2538.
- [10] Dahl, A. and Bonilla, E. V. (2018). Grouped gaussian processes for solar power prediction. *arXiv preprint arXiv:1806.02543*.
- [11] Dezfouli, A. and Bonilla, E. V. (2015). Scalable inference for Gaussian process models with black-box likelihoods. In *Neural Information Processing Systems*.
- [12] Evans, T. and Nair, P. (2018). Scalable gaussian processes with grid-structured eigenfunctions (gp-grief). In *International Conference on Machine Learning*, pages 1416–1425.
- [13] Gardner, J., Pleiss, G., Weinberger, K. Q., Bindel, D., and Wilson, A. G. (2018a). Gpytorch: Black-box matrix-matrix gaussian process inference with gpu acceleration. In *Advances in Neural Information Processing Systems*, pages 7587–7597.
- [14] Gardner, J. R., Pleiss, G., Wu, R., Weinberger, K. Q., and Wilson, A. G. (2018b). Product kernel interpolation for scalable Gaussian processes. *arXiv*, abs/1802.08903.
- [15] Genton, M. G. (2001). Classes of kernels for machine learning: a statistics perspective. *Journal of machine learning research*, 2(Dec):299–312.
- [16] Hensman, J., Matthews, A., and Ghahramani, Z. (2015). Scalable variational Gaussian process classification. In *AISTATS*.
- [17] Hensman, J., Rattray, M., and Lawrence, N. D. (2014). Fast nonparametric clustering of structured time-series. *IEEE Transactions on Pattern Analysis and Machine Intelligence*.
- [18] Kingma, D. P. and Ba, J. (2014). Adam: A method for stochastic optimization. *CoRR*, abs/1412.6980.
- [19] Quinero-Candela, J. and Rasmussen, C. E. (2005). Analysis of some methods for reduced rank gaussian process regression. In *Switching and learning in feedback systems*, pages 98–127. Springer.
- [20] Quiñero-Candela, J. and Rasmussen, C. E. (2005). A unifying view of sparse approximate Gaussian process regression. *JMLR*, 6:1939–1959.
- [21] Quiñero-Candela, J., Rasmussen, C., and Williams, C. (2007). *Approximation Methods for Gaussian Process Regression*, pages 203–223. Neural Information Processing. MIT Press, Cambridge, MA, USA.
- [22] Rasmussen, C. E. and Williams, C. K. I. (2006). *Gaussian processes for machine learning*. The MIT Press.
- [23] Rue, H., Martino, S., and Chopin, N. (2009). Approximate Bayesian inference for latent Gaussian models by using integrated nested Laplace approximations. *Journal of the royal statistical society: Series b (statistical methodology)*, 71(2):319–392.
- [24] Snelson, E. and Ghahramani, Z. (2006). Sparse Gaussian processes using pseudo-inputs. In *Neural Information Processing Systems*.
- [25] Solin, A. and Särkkä, S. (2014). Hilbert space methods for reduced-rank gaussian process regression. *arXiv preprint arXiv:1401.5508*.
- [26] Sun, D. and Sun, X. (2005a). Estimation of the multivariate normal precision and covariance matrices in a star-shape model. *Annals of the Institute of Statistical Mathematics*, 57(3):455–484.
- [27] Sun, X. and Sun, D. (2005b). Estimation of the cholesky decomposition of the covariance matrix for a conditional independent normal model. *Statistics & probability letters*, 73(1):1–12.

- [28] Teh, Y. W., Seeger, M., and Jordan, M. I. (2005). Semiparametric latent factor models. In *Artificial Intelligence and Statistics*.
- [29] Tipping, M. E. (2001). Sparse bayesian learning and the relevance vector machine. *J. Mach. Learn. Res.*, 1:211–244.
- [30] Titsias, M. (2009). Variational learning of inducing variables in sparse Gaussian processes. In *AISTATS*.
- [31] Voyant, C., Notton, G., Kalogirou, S., Nivet, M.-L., Paoli, C., Motte, F., and Fouilloy, A. (2017). Machine learning methods for solar radiation forecasting: A review. *Renewable Energy*, 105:569 – 582.
- [32] Whittaker, J. (2009). *Graphical models in applied multivariate statistics*. Wiley Publishing.
- [33] Widen, J., Carpman, N., Castellucci, V., Lingfors, D., Olauson, J., Remouit, F., Bergkvist, M., Grabbe, M., and Waters, R. (2015). Variability assessment and forecasting of renewables: A review for solar, wind, wave and tidal resources. *Renewable and Sustainable Energy Reviews*, 44:356–375.
- [34] Wilson, A. and Nickisch, H. (2015). Kernel interpolation for scalable structured gaussian processes (kiss-gp). In *International Conference on Machine Learning*, pages 1775–1784.
- [35] Wilson, A. G., Knowles, D. A., and Ghahramani, Z. (2012). Gaussian process regression networks. In *International Conference on Machine Learning*.
- [36] Yang, D., Kleissl, J., Gueymard, C. A., Pedro, H. T., and Coimbra, C. F. (2018). History and trends in solar irradiance and pv power forecasting: A preliminary assessment and review using text mining. *Solar Energy*.
- [37] Zhang, L., Zhou, W., and Jiao, L. (2004). Wavelet support vector machine. *IEEE Transactions on Systems, Man, and Cybernetics, Part B (Cybernetics)*, 34(1):34–39.